Effect of Inductance Ratio on Operating Frequencies of a Hybrid Resonant Inverter

Mojtaba Ghodsi, Hamidreza Ziaifar, Morteza Mohammadzaheri, Payam Soltani

Abstract—In this paper, the performance of a medium power (25 kW/25 kHz) hybrid inverter with a reactive transformer is investigated. To analyze the sensitivity of the inverster, the RSM technique is employed to manifest the effective factors in the inverter to minimize current passing through the Insulated Bipolar Gate Transistors (IGBTs) (current stress). It is revealed that the ratio of the axillary inductor to the effective inductance of resonant inverter (N), is the most effective parameter to minimize the current stress in this type of inverter. In practice, proper selection of N mitigates the current stress over IGBTs by five times. This reduction is very helpful to keep the IGBTs at normal temperatures.

Keywords—Analytical analysis, hybrid resonant inverter, reactive transformer, response surface method.

I. Introduction

IN the last decade, development of high speed and high power switches promise many applications for full-bridge inverters. AC drivers, non-destructive ultrasonic tests [1], linear direct-drive motors [2], induction heaters and switching power supplies for transducers are the most applications of the full bridges. Piezo elements, electrostatic, and magnetostrictive are the most popular techniques to develop miniature transducers that need the full-bridge inverters. Piezoelectric transducers [3]-[10] and electrostatic motors [11], [12] are capacitive loads. However, magnetostrictive transducers [13]-[27] are considered as inductive loads that need special consideration in their driving. Induction heaters are normally categorized based on the arrangement of their resonant tank topologies (Table I). Usually, induction heaters consist of a resonant tank that is in series or parallel to the heating coil, which is suitable for blazing, welding, and melting of metals. In all of the applications mentioned above, the full-bridge circuit is used to obtain a strong alternating magnetic field in the coil. Qi and Peng described the selection procedure of the series resonant inverter (SRI) [28] and Liu presented a fine-tuning technique to reduce the high voltage oscillation across the primary of the transformer in SRI [29]. Teeb and Hobson proposed a filter to eliminate the ringing problem made by switches in the parallel resonant inverter (PRI) [30]. Furthermore, Espi developed a highly efficient induction heater (25 kW/50 kHz) by PRI [31]. Espi and his team tried to enhance the performance of PRI and proposed a new hybrid resonant inverter (L-LC) to have the advantages of both SRI and PRI [32]-[34]. Borage also tried to signify the effect of the auxiliary inductor on the source current [35].
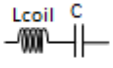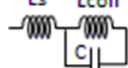
Mojtaba Ghodsi is with the School of Energy and Electronic Engineering, University of Portsmouth, UK (corresponding author, phone: +44 (0) 23 9284 2674; e-mail: mojtaba.ghodsi@port.ac.uk).
Hamidreza Ziaiefar and Morteza Mohammadzaheri are with Mechanical and Industrial Engineering Department, Sultan Qaboos University, P.O.Box 33, Alkhoud, Seeb, Muscat, Oman.
Payam Soltani is with School of Mechanical, Aerospace and Automatic Engineering, Coventry University, UK.

TABLE I
COMPARISON OF RESONANT TANK TOPOLOGIES

	Series	Parallel	Hybrid (L-LC)
Resonant tank topology			
Advantages	-Simple structure -Inexpensive	-Able to handle short circuit in the heating coil -Low current stress over switches - High voltage capacitor is not required	-Able to handle short circuit in heating coil (almost load independent) -Low current stress over switches - High voltage capacitor is not required for active transformer type -Suitable for high Q-factor applications
Disadvantages	-Not able to handle short circuit capability -High current stress over switches	-Big size	-High voltage capacitor is required for reactive transformer type
Applications	-Induction heater: e.g., warming, forging and rolling	-Induction heater: e.g., surface hardening	-Induction heater: e.g. (active transformer) tube welding, grain growing

In this paper, a technique to optimize the inductance to signify the effect of the auxiliary inductor on the source current value for an auxiliary inductor is presented to reduce current stress on the switches using the response surface method (RSM).

II. Principle and Analysis of Hybrid Resonance Inverter (L-LC)

A. Principle of Operation

As shown in Fig. 1, a 3- phase AC power source is rectified to provide a low ripple DC voltage. Four high-power IGBTs (Q_1, Q_2, Q_3, and Q_4) are employed to be derived by pulse width modules (PWM) in a way to generate a square waveform of voltage across *a-c*. The generated square waveform is fed to an axillary inductor (L_s) that is in series with a PRI. The PRI consists of a capacitor tank (C), which is parallel to the primary of a reactive transformer (T_p). The transformer is used for frequency matching and its secondary is connected to the heating coil.

By considering magnetic flux leakage in both primary and

World Academy of Science, Engineering and Technology
International Journal of Energy and Power Engineering
Vol:14, No:5, 2020

secondary coils, the transformer can be modeled as a combination of an ideal transformer and some equivalent resistors and inductors in primary and secondary [36]. After simplifying the circuits, its electrical equivalent circuit can be presented as in Fig. 3, as a hybrid inverter or L-LC inverter. The biggest advantage of the hybrid inverter is this point that large current will pass through the resonant tank (capacitor and primary of the transformer) while small current is demanded from a rectified DC source (Vcc). Therefore, small current (I_s) passes through the auxiliary inductor and IGBTs and enhances the lifetime of the IGBTs.
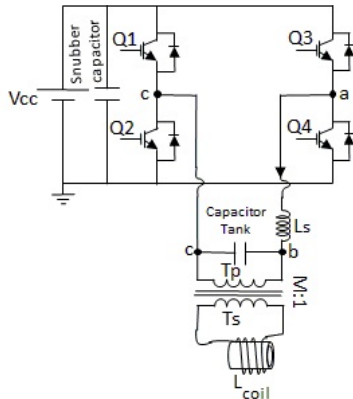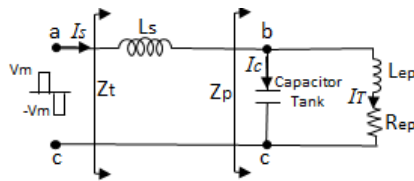

Fig. 1 Schematic of L-LC circuit

Fig. 2 Electrical equivalent circuit of L-LC

B. Analysis of Steady Sate Operation

As shown in Fig. 2, the impedance of the parallel ending circuit and total circuits after IGBTs are presented by Z_p and Z_t. The impedances, Z_p, and Z_t that are frequency-dependent can be calculated easily as:

$$Z_p = Z_c \parallel (Z_{Lep} + R_{ep}) \qquad (1)$$

$$Z_t = Z_{Ls} + Z_c \parallel (Z_{Lep} + R_{ep}) \qquad (2)$$

where $Z_{LS} = j\omega L_s$ and $Z_c = 1/j\omega C$ are the impedance of the inductor and capacitor tank. $Z_{Lep} = j\omega L_{ep}$ and R_{ep} are the equivalent impedance and resistance of primary by considering secondary coil effect. By simplifying (1) and (2), Z_p and Z_t can be rewritten in the following configurations:

$$Z_p(\omega) = \frac{R_{ep} + L_{ep}\omega j}{1 + L_{ep}C\omega^2 + RC\omega j} \qquad (3)$$

$$Z_t(\omega) = \frac{(R_{ep} - L_s R_{ep} C\omega^2) + [(L_{ep} + L_s)\omega - L_{ep}L_sC\omega^3]j}{1 - L_{ep}C\omega^2 + RC\omega j} \qquad (4)$$

where, C is the capacitance of the tank. From the characteristic equation of (3), the resonance frequency of the parallel ending is ω_p, which is:

$$\omega_p = \frac{1}{\sqrt{L_{ep}C}} \qquad (5)$$

Since IGBTs (Q_1, Q_2, Q_3, and Q_4) are energized by PWM, a square shape waveform by the amplitude of V_m is generated across a-c. Based on the Fourier series, the amplitude of its first harmonic is:

$$V_1 = \frac{4V_m}{\pi} \qquad (6)$$

Therefore, approximately the average electrical power transmitted to the circuit from input can be calculated as:

$$P(\omega) = \frac{V_1^2}{2 \times abs\,(Z_t(\omega))} \qquad (7)$$

By minimizing the absolute value of the Z_t that is the denominator of (7), the maximum power is achievable at ω_0 by:

$$\omega_0 = \frac{1}{\sqrt{LC}} \qquad (8)$$

where,

$$L = L_s \parallel L_{ep} = \frac{L_s L_{ep}}{L_s + L_{ep}} = \frac{L_{ep}}{1 + \frac{L_{ep}}{L_s}} = \frac{L_{ep}}{1 + \frac{1}{N}} \qquad (9)$$

and N is the ratio of L_s to L_{ep}. Since L is always smaller than L_{ep}, then always $\omega_p < \omega_0$. After finding the resonance frequency of circuit, ω_0, the current gain can easily be obtained by combining (10) and (11).

$$I_T(Z_{Lep} + R_{ep}) = I_C Z_c \qquad (10)$$

$$I_T + I_C = I_s \qquad (11)$$

then,

$$H(\omega) = \frac{I_T}{I_s} = \frac{1}{1 - L_{ep}C\omega^2 + R_{ep}C\omega j} \qquad (12)$$

and,

$$|H(\omega)|^2 = \left|\frac{I_T}{I_s}\right|^2 = \frac{1}{(1 - L_{ep}C\omega^2)^2 + (R_{ep}C\omega)^2} \qquad (13)$$

Higher H shows less current stress on the IGBTs while large current passing through the transformer. Normally, the circuit is tuned in resonance frequency, ω_0, to operate in the maximum power. By substituting (8) in (13), H value in resonance frequency is provable by:

$$|H(\omega)|_{\omega=\omega_0} = \frac{Q}{\sqrt{1 + \left(\frac{Q}{N}\right)^2}} \qquad (14)$$

where Q is the quality factor and shows the ratio of reactive power to active power. Q of L-LC circuit is achievable by:

World Academy of Science, Engineering and Technology
International Journal of Energy and Power Engineering
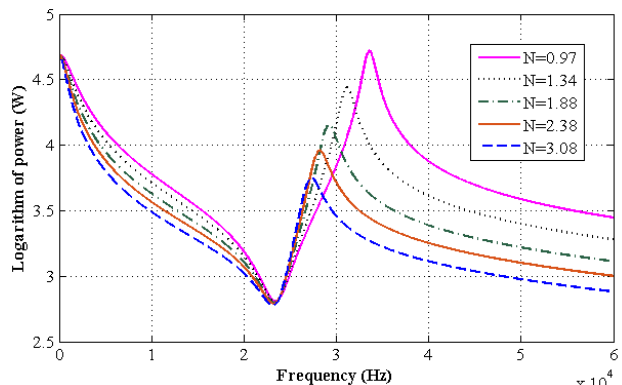Vol:14, No:5, 2020

$$Q^2 = \frac{L}{R_{ep}^2 C} \qquad (15)$$

Thanks to compressing form of Q total impedance at resonance, $Z_t(\omega_0)$, can be derived from (16):
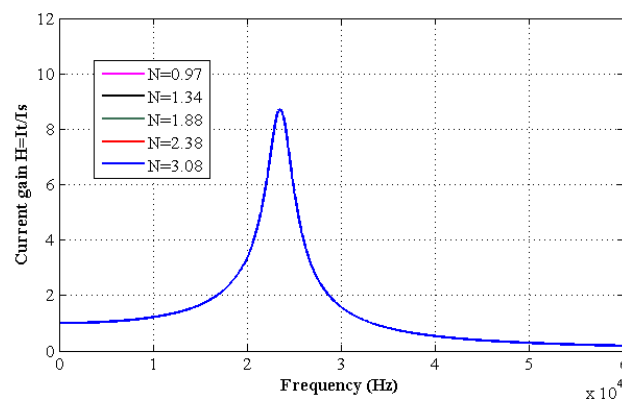
$$Z_t(\omega_0) = \frac{N^2 L_{ep} \omega_0}{Q - j(N+1)} \qquad (16)$$
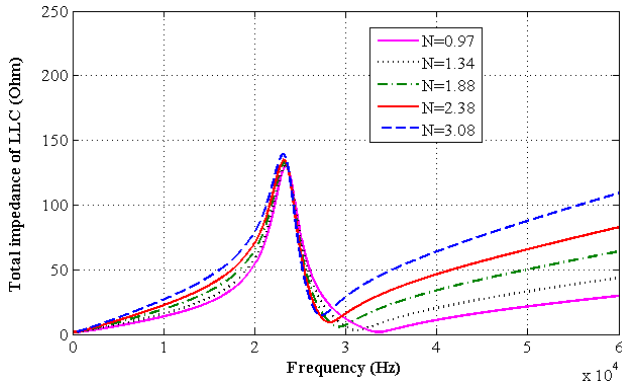

(a)

(b)

(c)

Fig. 3 Effect of N by changing L_s on (a) total impedance of L-LC circuit (b) power (c) current gain

It can be concluded from (16) that L-LC is not a purely resistive load and IGBTs IGBTs (Q_1, Q_2, Q_3, and Q_4) before the LLC circuit (Fig. 1) must tolerate reactive current. To reduce this reactive current, $Z_t(\omega_0)$ must be close to the characteristic of a resistive load. Therefore, the argument of $Z_t(\omega_0)$, called "switching angle", needs to be as small as possible. The switching angle, ϕ, can be calculated from (17).
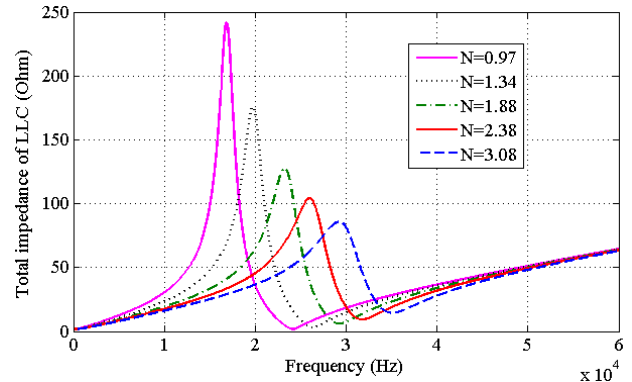
(a)
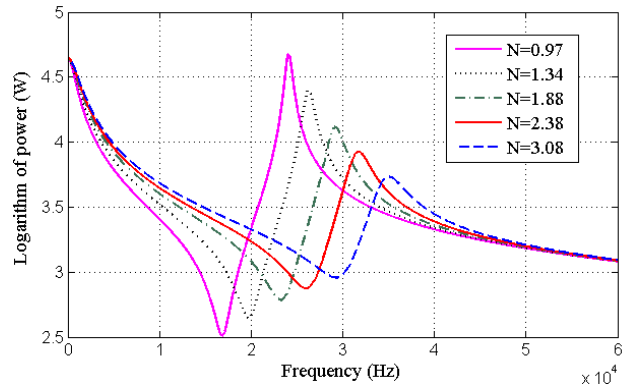
(b)
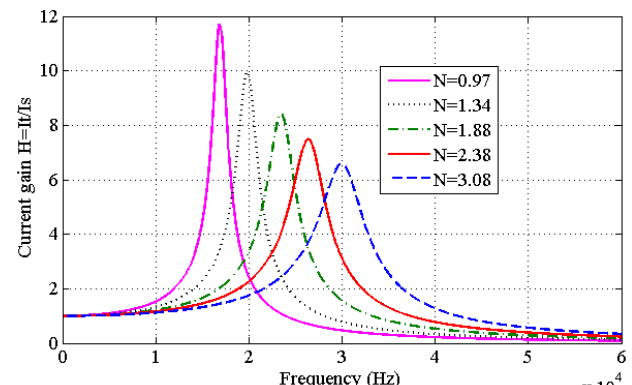
(c)

Fig. 4 Effect of N by changing L_T on (a) total impedance of L-LC circuit (b) power (c) current gain

For better performance of the IGBTs, it is recommended to have ϕ less than $\pi/9$ rad [14]. It will be illustrated later that for small Q (Q <10) it is better to have small N.
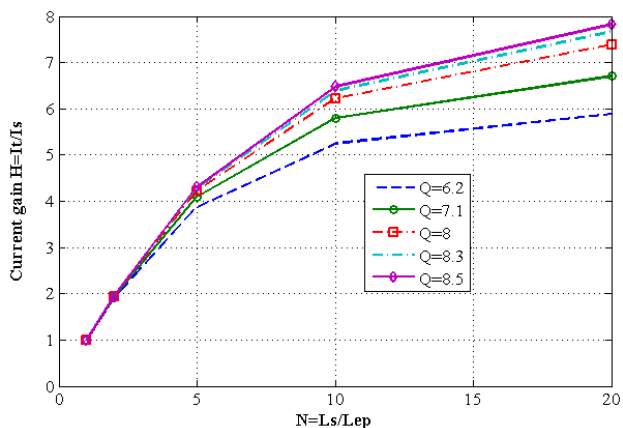
$$\phi = \arg[Z_t(j\omega_0)] = \tan^{-1}\left(\frac{N+1}{Q}\right) \qquad (17)$$

World Academy of Science, Engineering and Technology
International Journal of Energy and Power Engineering
Vol:14, No:5, 2020

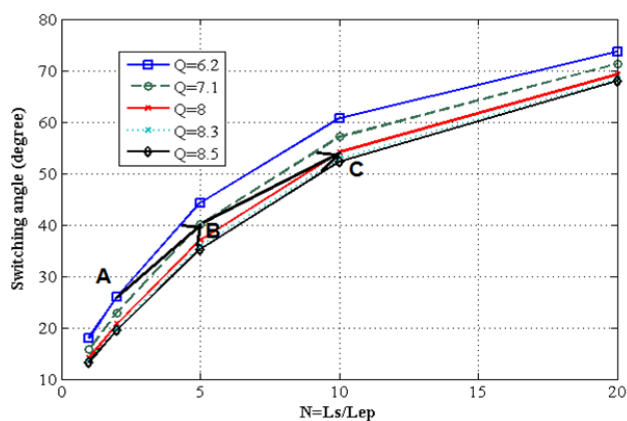Fig. 5 Relationship between H and N in various Q_0

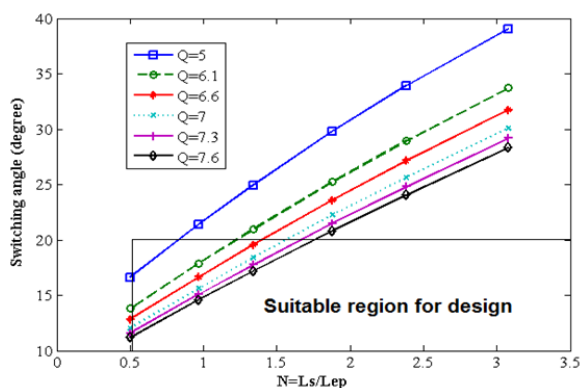Fig. 6 Relationship between ϕ and N in various Q

Fig. 7 Effect of N on and N (smaller range of N) in various Q

As shown in Fig. 3, the equivalent total impedance of the LLC circuit reaches its maximum value in ω_p and reduces to its minimum value at ω_0, where the power is in its maximum value (Fig. 4). As it is diagnosable from (13), a variation of N does not affect parallel frequency (ω_p) while it changes resonance frequency, ω_0. To retain operation in the highest power point, a self-tuning control system modifies operation resonance frequency. Figs. 4 and 5 disclose this fact that lower N causes higher resonance frequency and lower H. Moreover, Fig. 6 confirms the effect of N on the current stress, H, at the resonance frequency. The enhancement of H, by increasing N and Q is predictable from (14). As shown in Fig. 7, the direction of modification by increasing N is from point A towards point B and C. Nevertheless, with the current gain and quality factor, Q, increasing by N, the switching angle (Fig. 7) will increase and heat generation in the IGBTs abates the lifetime of switches. It is vital to keep the switching angle at fewer than 20 degrees. In other words, a smaller N is preferable. Fig. 8 concentrates on small N values. It is clear that N > 1.7 is not recommended since its switching angle exceeds 20° [34].

III. OPTIMIZATION USING RESPOND SURFACE METHOD

Design and analysis of the experiment (DOE) is one of the fruitful tools to opt the significant factors in any test. To optimize any objective in any experiment, RSM, which is a combination of mathematical and statistical techniques, can be employed [2], [37]. The objective or response of interest in some experiments is a function of several variables or factors. Good modeling, few numbers of initial experiments combined with a fast analyzing process present RSM as an appropriate approach for optimizing this response of interest. Modeling by RSM means a presentation of a mathematical relationship between variables and objective as an output. For example, in this paper, we would like to select the proper values for element values of the hybrid inverter for warming applications to minimize current stress over its IGBTs. After manufacturing the inverter, the current stress over its IGBTs is measured.
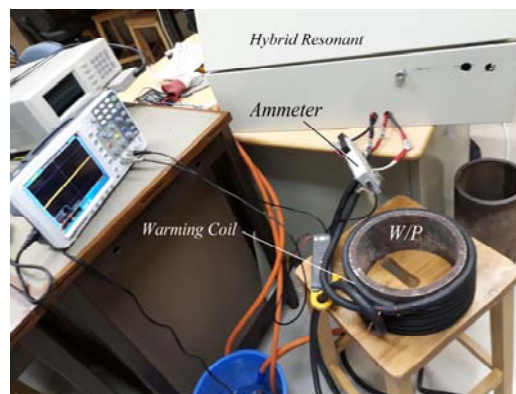
Fig. 8 The developed induction heater

TABLE II
CODED INPUT VARIABLES (FACTORS)

Factors	Unit	-α	-1	0	+1	+☐
Vcc	V	23	27	37	47	51
N	--	0.77	1.04	1.43	1.81	2.33

By analyzing these results using RSM, the proper values for elements will be selected. The aim of this section is the enhancement of the current gain. In other words, H value is selected as the cost function or objective. It seems that all elements in the L-LC circuit play an important role in current stress. As mentioned in (14), it seems that H depends on Q and N. Furthermore, initial observations show that H depends on V_{cc} too. Since Q depends on L, C and R_{ep} and C and R_{ep} are

World Academy of Science, Engineering and Technology
International Journal of Energy and Power Engineering
Vol:14, No:5, 2020

constant, then Q depends on L. Therefore, H is considered as output and N and V_{cc} considered as the effective factors. Analyzing with RSM starts by finding the mathematical relationship between inputs and output. In this research, the design of experiments is based on the central composite design (CCD). Minitab 17 software is employed to find a linear regression equation. Table II shows two factors with five levels. Based on the design by RSM and selecting of α=1.141, it is noticed that 13 experiments by manufactured prototype including five center points are required (Table III). Measurements are performed randomly and the results are presented in Table III.

TABLE III
SIMULATIONS RESULTS BASED ON RSM AT RESONANCE CONDITION

Order of Run	V_{cc} (V)	L_s/L_{ep}	$H=I_T/I_S$
1	-1	-1	1.091
4	+1	+1	3.842
5	-1.414	0	2.083
13	0	0	5.179
11	0	0	4.567
6	1.414	0	4.054
3	-1	+1	2.857
10	0	0	4.143
12	0	0	4.256
8	0	+1.414	4.48
9	0	0	3.847
2	+1	-1	1.375
7	0	-1.414	0.967

TABLE IV
COEFFICIENT OF THE REGRESSION EQUATION AND P-VALUE IN INITIAL AND MODIFIED MODELS

Terms	Initial Model		Modified Model	
	Reg. Eq. Coefficient	P_{value}	Reg. Eq. Coefficient	P_{value}
Constant	4.039	0.000	2.955	0.000
V_{cc}	0.462	0.193	1.105	0.018
N	1.105	0.016	-------	------
V_{cc}^2	-0.659	0.132	-----	------
N^2	-0.832	0.072	-----	-----
$V_{cc}*N$	0.085	0.852	-----	-----

TABLE V
SPECIFICATION OF DEVELOPED INVERTER

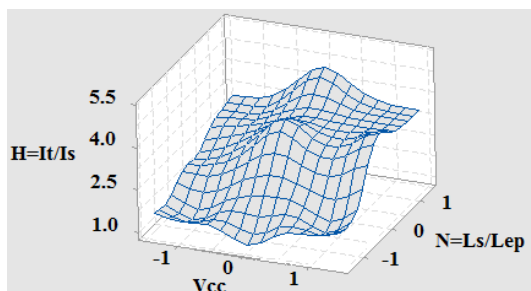| Designed parameters	Values
Transformer secondary inductance, L_{ep}	100 μH
Capacitor tank, C	0.454 μF
IGBT switches	1200 V, 200 A

Fig. 9 The relationship between H, Vcc and N

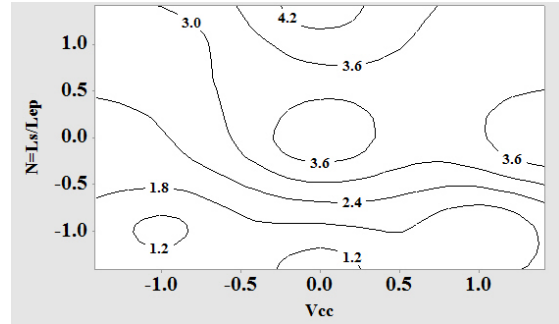Fig. 10 Contour plot of H vs.Vcc and N

Table IV presents the initial model, modified model, elimination of insignificant factors and coefficients of the regression equation. It is necessary to add that the factors with P_{value} less than 0.05 are effective on the output with 95% reliability. Regarding the coefficients presented in Table IV, the current gain can be modeled by (18):

$$H = 2.955 + 1.105\,N \qquad (18)$$

A. Influence of Input Voltage (V_{cc})

The specifications of used elements in the developed hybrid inverter (Fig. 9) are mentioned in Table V. Initial tests show that V_{cc} is effective on H. Although larger V_{cc} causes a higher current in the system, its P_{value} is more than 0.05. It means V_{cc} does not affect the current gain. This result is predictable from (13).

B. Influence of Ration of Axillary Inductance to Transformer Inductance (N)

The P_{value} of N shows that N is effective on H (Table IV). Figs. 9 and 10 plot the interaction between V_{cc} and N. It is visible that higher N causes higher H and it can reach to five. It means that current passing through the primary coil of the transformer is about five times that of the current passing through IGBT switches and causes less current stress on the IGBTs.

IV. CONCLUSION

In this paper, the performance of a medium power (25 kW, 25 kHz) hybrid inverter with a reactive transformer is investigated. To analyze the sensitivity of the inverter, the RSM technique is employed to highlight the effective factors in the inverter to maximize/minimize current gain/stress passing through the IGBTs. It is demonstrated that the ratio between axillary inductor to the effective inductance of resonant inverter (N) is the most effective parameter to minimize the current stress in this type of inverter. Higher N causes less current stress. However, there is a trade-off between N and the switching angle. It is revealed that the switching angle must be kept less than 20°. In practice, the current stress is reduced about five-fold in the IGBTs, which is very useful to enhance the lifetime of IGBTs.

REFERENCES

[1] J. Li, W. An, H. Gao, Y. Zhao, and Y. J. A. O. S. Sun, "An experimental

World Academy of Science, Engineering and Technology
International Journal of Energy and Power Engineering
Vol:14, No:5, 2020

study on oil droplet size distribution in subsurface oil releases," vol. 37, pp. 88-95, 2018.

[2] M. Ghodsi, "Optimization of mover acceleration in DC tubular linear direct-drive machine using response surface method," International Review of Electrical Engineering, vol. 10, pp. 492-500, 2015.

[3] H. Hoshyarmanesh, M. Ghodsi, and H.-H. Park, "Electrical properties of UV-irradiated thick film piezo-sensors on superalloy IN718 using photochemical metal organic deposition," Thin Solid Films, vol. 616, pp. 673-679, 2016.

[4] H. Hoshyarmanesh, N. Nehzat, M. Salehi, and M. Ghodsi, "X-ray diffraction measurement of residual stress in sol-gel grown lead zirconate titanate thick films on nickel-based super alloy substrate," Journal of Mechanical Science and Technology, vol. 29, pp. 715-721, 2015.

[5] H. Hoshyarmanesh, N. Nehzat, M. Salehi, M. Ghodsi, H.-S. Lee, and H.-H. Park, "Piezoelectric Transducers on Curved Dispersive Bending Wave and Poke-Charged Touch Screens," Materials and Manufacturing Processes, vol. 29, pp. 870-876, 2014.

[6] H. Hoshyarmanesh, N. Nehzat, M. Salehi, M. Ghodsi, H.-S. Lee, H.-H. Park, et al., "Thickness and thermal processing contribution on piezoelectric characteristics of Pb (Zr-Ti) O3 thick films deposited on curved IN738 using sol–gel technique," Proceedings of the Institution of Mechanical Engineers, Part L: Journal of Materials: Design Applications vol. 229, pp. 511-521, 2015.

[7] M. Mohammadzaheri, M. Emadi, M. Ghodsi, E. Jamshidi, I. Bahadur, A. Saleem, et al., "A variable-resistance digital charge estimator for piezoelectric actuators: An alternative to maximise accuracy and curb voltage drop," Journal of Intelligent Material Systems and Structures, vol. 30, pp. 1699-1705, 2019.

[8] S. Ghorbanirezaei, Y. Hojjat, and M. Ghodsi, "Design and fabrication of a new piezoelectric paper feeder actuator without mechanical parts," Smart Structures and Systems, vol. 24, pp. 183-191, 2019.

[9] H. Hoshyarmanesh, A. Abbasi, P. Moein, M. Ghodsi, and K. Zareinia, "Design and Implementation of an Accurate, Portable, and Time-Efficient Impedance-Based Transceiver for Structural Health Monitoring," IEEE/ASME Transactions on Mechatronics, vol. 22, pp. 2809-2814, 2017.

[10] H. Sadeghian, Y. Hojjat, M. Ghodsi, and M. R. Sheykholeslami, "An approach to design and fabrication of a piezo-actuated microdroplet generator," The International Journal of Advanced Manufacturing Technology, vol. 70, pp. 1091-1099, 2014.

[11] M. Modabberifar, M. Ghodsi, and Y. Hojjat, "Analysis of parameter effects on electrostatic induction dielectric sheet conveyor performance," International Journal of Precision Engineering Manufacturing, vol. 13, pp. 65-70, 2012.

[12] M. Dadkhah, Y. Hojjat, J. Jeon, M. Ghodsi, and M. Modabberifar, "Voltage-induction synchronous electrostatic motor," The International Journal of Advanced Manufacturing Technology, vol. 77, pp. 145-164, 2015.

[13] M. Ghodsi, T. Ueno, H. Teshima, H. Hirano, T. Higuchi, and E. Summers, ""Zero-power" positioning actuator for cryogenic environments by combining magnetostrictive bimetal and HTS," Sensors and Actuators A: Physical, vol. 135, pp. 787-791, 2007.

[14] M. Ghodsi and M. Modabberifar, "Quality factor, static and dynamic responses of miniature galfenol actuator at wide range of temperature," International Journal of Physical Sciences, vol. 6, pp. 8143-8150, 2011.

[15] M. Ghodsi, T. Ueno, and T. Higuchi, "Novel Magnetostrictive Bimetal Actuator Using Permendur," Advanced Materials Research, vol. 47-50, pp. 262-265, 2008.

[16] M. Ghodsi, N. Hosseinzadeh, A. Ozer, H. R. Dizaj, Y. Hojjat, N. G. Varzeghani, et al., "Development of Gasoline Direct Injector Using Giant Magnetostrictive Materials," IEEE Transactions on Industry Applications, vol. 53, pp. 521-529, 2017.

[17] M. R. Karafi, M. Ghodsi, and Y. Hojjat, "Development of Magnetostrictive Resonant Torsional Vibrator," IEEE Transactions on Magnetics, vol. 51, pp. 1-8, 2015.

[18] M. R. Karafi, Y. Hojjat, F. Sassani, and M. Ghodsi, "A novel magnetostrictive torsional resonant transducer," Sensors and Actuators A: Physical, vol. 195, pp. 71-78, 2013.

[19] M. Sheykholeslami, Y. Hojjat, M. Ghodsi, K. Kakavand, and S. Cinquemani, "Investigation of ΔE Effect on Vibrational Behavior of Giant Magnetostrictive Transducers," Shock and Vibration, vol. 2015, pp. 1-9, 2015.

[20] M. R. Sheykholeslami, Y. Hojjat, S. Cinquemani, M. Ghodsi, and M. Karafi, "An approach to design and fabrication of resonant giant

[21] M. Sheykholeslami, Y. Hojjat, M. Ghodsi, M. Zeighami, and K. Kakavand, "Effect of magnetic field on mechanical properties in Permendur," Materials Science and Engineering: A, vol. 651, pp. 598-603, 2016.

[22] S. Talebian, Y. Hojjat, M. Ghodsi, and M. R. Karafi, "Study on classical and excess eddy currents losses of Terfenol-D," Journal of Magnetism and Magnetic Materials, vol. 388, pp. 150-159, 2015.

[23] S. Talebian, Y. Hojjat, M. Ghodsi, M. R. Karafi, and S. Mirzamohammadi, "A combined Preisach–Hyperbolic Tangent model for magnetic hysteresis of Terfenol-D," Journal of Magnetism Magnetic Materials, vol. 396, pp. 38-47, 2015.

[24] M. Ghodsi, H. Ziaiefar, K. Alam, M. Mohammadzaheri, A. Al-Yahmedi, and F. K. Omar, "Electromechanical Modelling and Experimental Verification of Cantilevered Permendur Energy Harvester," presented at the IEEE/ASME International Conference on Advanced Intelligent Mechatronics, 2018.

[25] M. Ghodsi, H. Ziaiefar, M. Mohammadzaheri, and A. Al-Yahmedi, "Modeling and Characterization of Permendur Cantilever Beam for Energy Harvesting," Energy, vol. 176, pp. 561-569, 2019.

[26] M. Ghodsi, H. Ziaiefar, M. Mohammadzaheri, and A. Al-Yahmedi, "Development of Magnetostrictive Harvester for Unmanned Aerial Vehicles (UAV)," in 2019 1st International Conference on Unmanned Vehicle Systems-Oman (UVS), 2019, pp. 1-6.

[27] M. Ghodsi, H. Ziaifar, M. Mohammadzaheri, and P. Soltani, "Effect of Damping on Performance of Magnetostrictive Vibration Energy Harvester," International Journal of Mechanical and Mechatronics Engineering, vol. 14, pp. 147-151, 2020.

[28] X. Qi, Y. Peng, and Y. Li, "Parameters design of series resonant inverter circuit," Physics Procedia, vol. 24, pp. 133-138, 2012.

[29] L.-j. Liu, K.-x. Yu, M. Zhang, J.-y. Nan, G.-z. Jiang, B. Rao, et al., "Analysis on voltage oscillation of a mid-frequency series resonant inverter for DRMP coils on J-TEXT," Fusion Engineering and Design, vol. 102, pp. 59-65, 2016.

[30] D. Tebb and L. Hobson, "Design of matching circuitry for 100-kHz MOSFET induction heating power supply," IEEE Transactions on Industrial Electronics, pp. 271-276, 1987.

[31] E. J. Dede, J. V. Gonzalez, J. A. Linares, J. Jordan, D. Ramirez, and P. Rueda, "25-kW/50-kHz generator for induction heating," IEEE transactions on industrial electronics, vol. 38, pp. 203-209, 1991.

[32] J. Espi, E. Dede, A. Ferreres, and R. Garcia, "Steady-state frequency analysis of the" LLC" resonant inverter for induction heating," in V IEEE International Power Electronics Congress Technical Proceedings, CIEP 96, 1996, pp. 22-28.

[33] J. Espi and E. Dede, "Design considerations for three element L-LC resonant inverters for induction heating," International journal of electronics, vol. 86, pp. 1205-1216, 1999.

[34] J. M. Espi-Huerta, E. J. D. G. Santamaria, R. G. Gil, and J. Castello-Moreno, "Design of the L-LC resonant inverter for induction heating based on its equivalent SRI," IEEE transactions on industrial electronics, vol. 54, pp. 3178-3187, 2007.

[35] M. Borage and S. Tiwari, "A 25 kW, 25 kHz induction heating power supply for MOVPE system using L-LC resonant inverter," Advances in Power Electronics, vol. 2013, 2013.

[36] K. Shaarbafi, "Transformer modelling guide," Alberta Electric System Operator (AESO), Tech. Rep, 2014.

[37] M. Ghodsi, H. Ziaiefar, M. Mohammadzaheri, F. K. Omar, and I. Bahadur, "Dynamic analysis and performance optimization of permendur cantilevered energy harvester," Smart Structures and Systems, vol. 23, pp. 421-428, 2019.